J. Fluid Mech. (1996), *vol.* 325, *pp.* 331–355

Transport in lungs and branched estuaries

By RONALD SMITH

Mathematical Sciences, Loughborough University, LE11 3TU, UK

(Received 29 September 1995 and in revised form 24 May 1996)

Longitudinal mass transport in branched oscillatory flows is greater than in non-branched oscillatory flows. Here a derivation is given of a longitudinal diffusion equation which governs the long-term mass transport when there is perfect synchronism of the flow in adjacent branches. An explicit formula is obtained for the shear dispersion coefficient (effective longitudinal diffusion) when a sinusoidal flow excursion crosses a junction in geometrically self-similar flows with negligible secondary flow. A single junction crossing can be sufficient to double the shear dispersion as compared to an unbranched flow at the same frequency.

1. Introduction

High-frequency ventilation of the lungs offers the prospect of a gentle yet efficient means of respiration during surgery, with particular advantages for premature babies whose immature lungs are not very flexible (Bohn *et al.* 1980; Rossing *et al.* 1981). This prospect has led to a large number of experimental investigations *in vivo* and *in vitro*, concerned with understanding, calibrating and optimizing the efficiency. Existing theories for oscillatory dispersion in straight tubes (Chatwin 1975; Watson 1983) have been used as an aid in the scaling and interpretation of results. The key feature is that for branched flows the effective longitudinal mixing rates are systematically higher than for the corresponding non-branched flows (Paloski, Slosberg & Kamm 1987, figure 7).

For steady river flows with branches and with islands Daish (1985) and Smith (1995), respectively, have calculated similar high local shear dispersion coefficients. They point out that it takes a substantial distance along a branch for the junction-induced distortion of the concentration profile across the flow to adjust to the new geometry. It is this additional distortion that leads to the shear dispersion exceeding the non-branched value. Flow oscillations, in estuaries or lungs, could inhibit the distortion and related dispersion by reversing more rapidly than the cross-sectional mixing time (Chatwin 1975; Watson 1983). So, the present calculations focus upon regimes in which neither the flow excursions nor the cross-sectional mixing rate can be neglected.

The outcome of the first half of this paper is a diffusion equation along the branched network for the cycle-averaged concentration. The effective diffusivity varies throughout the network and depends upon the across-flow distortion experienced locally within a single flow excursion. For estuaries there is also a mean drift associated with fresh-water inflow from rivers. The evaluation of the across-flow distortion (and consequent shear dispersion coefficient) for a class of branching flows is achieved in the second half of this paper. A simple estuarial example is used to demonstrate the magnitude of the increased dispersion associated with branching.

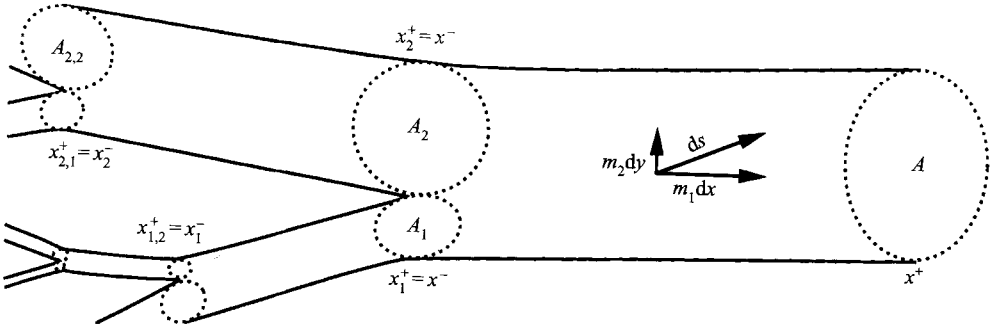

FIGURE 1. Definition sketch for metric coefficients and for the labeling of branches.

2. Interior volumes

The geometry of a branching flow system is a first major obstacle to any mathematical theory (Daish 1985; Smith 1995). In lungs and in estuaries the narrowness of the channels gives a clearly defined principal x-direction. To avoid the need for general tensor analysis, we assume that there is an orthogonal coordinate system (x, y, z). The metric coefficients m_1, m_2, m_3 relate the distance increment $\mathrm{d}s$ to the coordinate increments $\mathrm{d}x$, $\mathrm{d}y$, $\mathrm{d}z$ (see figure 1):

$$\mathrm{d}s^2 = m_1{}^2\mathrm{d}x^2 + m_2{}^2\mathrm{d}y^2 + m_3{}^2\mathrm{d}z^2 \,. \tag{2.1}$$

For example, in shallow water flows with depth-following coordinates, the bed and free surface would be designated $z = 0$ and $z = 1$. Hence, m_3 would be the time-dependent total water depth. If also $m_2 = B$, where $2B$ is the instantaneous width, then the banks could be $y = \pm 1$. For a network of flexible cylindrical tubes $y = r/a$ could be the fraction of the local radius $a(x, t)$ with $m_2 = a$ and $z = \theta$ the angular coordinate with $m_3 = ay$.

No index is needed to identify the outermost channel. Its inner and outer ends are denoted x^- and x^+ (see figure 1). Progressing inwards, at each junction we use an index i to label the channels along a branching route. If at N successive junctions the selection of channels is $i_1, i_2, \ldots, i_N$ then we can use the multi-index

$$\boldsymbol{\mu} = i_1, i_2, \ldots, i_N \quad \text{or} \quad \boldsymbol{\mu}_N = \boldsymbol{\mu}_{N-1}, i_N \tag{2.2}$$

to identify the channel (Smith 1995). We denote the longitudinal position of the inner and outer ends of a channel as $x_{\boldsymbol{\mu}}^-$, $x_{\boldsymbol{\mu}}^+$ with the obvious matching $x_{\boldsymbol{\mu}_N}^+ = x_{\boldsymbol{\mu}_{N-1}}^-$. The notation

$$\boldsymbol{\mu}' \leqslant \boldsymbol{\mu} \quad (\text{e.g.} \quad \boldsymbol{\mu}_{N+1} < \boldsymbol{\mu}_N) \tag{2.3}$$

is used to indicate that the multi-index $\boldsymbol{\mu}'$ is equal to or extends the multi-index $\boldsymbol{\mu}$. In physical terms, the channel $\boldsymbol{\mu}'$ is either the channel $\boldsymbol{\mu}$ itself or one of the tributaries inland (further into the lungs or to the left in figure 1) from the channel $\boldsymbol{\mu}$.

Within a channel we identify a cross-section as $\Omega_{\boldsymbol{\mu}}$. The derivative of the volume between adjacent x-contours is denoted

$$A_{\boldsymbol{\mu}} = \int_{\Omega_{\boldsymbol{\mu}}} m_1 m_2 m_3 \mathrm{d}y\mathrm{d}z = \int_{\Omega_{\boldsymbol{\mu}}} \mathrm{d}\Omega \,. \tag{2.4}$$

Averaging denoted by an overbar is defined:

$$\bar{u}_\mu = \frac{1}{A_\mu}\int_{\Omega_\mu} m_1 m_2 m_3 u \mathrm{d}y\mathrm{d}z = \frac{1}{A_\mu}\int_{\Omega_\mu} u \mathrm{d}\Omega \ . \tag{2.5}$$

The cross-sectional area is given by the product $A_\mu \overline{m_1^{-1}}$. For ease of interpretation, it is convenient if the derivative of the volume between adjacent x-contours is the same as the cross-sectional area, i.e. if $\overline{m_1^{-1}} = 1$. If so, then x has the natural interpretation as a distance coordinate, while the cross-sectional coordinates y, z remain at our disposal (to accommodate width, depth or shape changes with time or with position).

The instantaneous volume of water in a subsection of an estuary interior to a longitudinal position x in the particular channel μ (or volume of gas interior to part of the lungs) is the summation of the volume derivatives over all interior branches and in the channel μ out as far as the position x :

$$V_\mu(x,t) = \sum_{\mu'<\mu}\int_{\mu'} A_{\mu'}(x,t)\mathrm{d}x + \int_{x_\mu^-}^{x} A_\mu(x',t)\mathrm{d}x' \ . \tag{2.6}$$

The velocity of a frame of reference moving with fixed V_μ within a given channel μ will be denoted $u_\mu^{(0)}$. An immediate consequence is that

$$\partial_t V_\mu + u_\mu^{(0)}\partial_x V_\mu = 0 \ . \tag{2.7}$$

On moving outward across a junction from $x_{\mu_N}^+$ to $x_{\mu_{N-1}}^-$, the merging of channels (and merging of the associated interior volumes) causes a jump in the interior volume.

An infinite geometric series of individually straight, branching channels provides a particularly simple example. The length from alveolus to mouth is denoted L and the area just before the mouth is A. At each branching there is splitting into M sub-channels with area ratio α and length ratio Λ. At the Nth generation there are M^N identical channels all with area $\alpha^N A$ and length $\Lambda^N(1-\Lambda)L$. The tide going in (or inhalation) can be modelled by an increasing value of α, A, Λ or L. For the total volume to remain finite, the product $M\alpha\Lambda$ must be less than unity. Within each of the M^N members of the Nth generation, with $\Lambda^{N+1}L \leqslant x \leqslant \Lambda^N L$, the formula for the interior volume is

$$V_{\mu_N}(x,t) = M(\alpha\Lambda)^{N+1}\frac{(1-\Lambda)LA}{1-M\alpha\Lambda} + \alpha^N(x - L\Lambda^{N+1})A \quad . \tag{2.8}$$

3. Equations for flow and concentration

The rates at which the flow crosses the coordinate contours are denoted (u,v,w) and the corresponding velocity components, relative to any contour movement, are (m_1u, m_2v, m_3w). For gas at sub-acoustic frequencies and at pressures close to atmospheric, density changes are negligible. The incompressibility condition satisfied by the flow field is

$$\partial_t(m_1m_2m_3) + \partial_x(m_1m_2m_3u) + \partial_y(m_1m_2m_3v) + \partial_z(m_1m_2m_3w) = 0 \ . \tag{3.1}$$

At lateral boundaries the normal component of relative velocity equals that of the boundary. In practice it is convenient to select the metric coefficients m_1, m_2, m_3 so that the coordinate contours move with the boundary. If so, then the normal component of relative velocity would be zero. In the present paper we shall not be concerned with calculating the flow: it will be regarded as being given. However, the

constraint (3.1) upon the flow allows alternative formulations of the concentration equation.

Since we are assuming there is no flow through the lateral boundaries, the cross-sectionally averaged conservation of volume can be stated:

$$\partial_t(A_\mu) + \partial_x(A_\mu \bar{u}_\mu) = 0 \,. \tag{3.2}$$

It is an elementary consequence that

$$0 = A_\mu(\bar{u}_\mu - u_\mu^{(0)}) - \varepsilon Q_\mu = \text{ flux out } - \text{ flux in } , \tag{3.3}$$

where $\varepsilon Q_\mu(t)$ is the summation of the river volume fluxes (net gas volume flux across the alveoli) for those tributaries which eventually feed into the channel μ. The parameter ε will be used subsequently both to characterize the net volume fluxes as being small relative to the periodic flow oscillations and to characterize the narrowness of the channels.

If the principal values $\kappa_1, \kappa_2, \kappa_3$ for diffusion correspond to the x, y, z coordinate directions, then the advection-diffusion equation for the tracer concentration c can be written

$$\begin{aligned} &m_1 m_2 m_3 \left(\partial_t c + u\partial_x c + v\partial_y c + w\partial_z c\right) \\ &- \partial_x\left(\frac{m_2 m_3}{m_1}\kappa_1 \partial_x c\right) - \partial_y\left(\frac{m_1 m_3}{m_2}\kappa_2 \partial_y c\right) - \partial_z\left(\frac{m_1 m_2}{m_3}\kappa_3 \partial_z c\right) = 0. \end{aligned} \tag{3.4}$$

The normal flux across lateral boundaries is assumed to be zero. If at junctions the adjustment of the geometry and flow is rapid, compared with mixing across the channels, then it may be appropriate to use different coordinate systems in the different channels. If so, it is important that continuity of concentration is preserved by appropriate particle-following matching (superscripts $-$ or $+$ indicate the direction from old to new channel):

$$y_{\mu,i} = Y_{\mu,i}^{-}(y_\mu, z_\mu, t) \,, \quad z_{\mu,i} = Z_{\mu,i}^{-}(y_\mu, z_\mu, t) \,, \tag{3.5a,b}$$

or

$$y_\mu = Y_{\mu,i}^{+}(y_{\mu,i}, z_{\mu,i}, t) \,, \quad z_\mu = Z_{\mu,i}^{+}(y_{\mu,i}, z_{\mu,i}, t) \,. \tag{3.5c,d}$$

The incompressibility condition (3.1) allows the advected derivatives in equation (3.4) to be written in conservation form. The cross-sectionally averaged mass conservation equation is then

$$A_\mu(\partial_t \bar{c} + \bar{u}_\mu \partial_x \bar{c}) + \partial_x(A_\mu \overline{(c-\bar{c})(u-\bar{u}_\mu)}) - \partial_x\left(A_\mu \overline{\frac{\kappa_1}{m_1^2}\partial_x c}\right) = 0 \,. \tag{3.6}$$

In § 5 a Taylor (1953) type of solution is obtained for $(c - \bar{c})$ in terms of $\partial_x \bar{c}$. This would change (3.6) into an advection-diffusion equation. One of the key results of this paper (6.6), is a flow-splitting, volume-following, time-cycle-averaged version of (3.6).

4. Volume-following coordinate

Another major obstacle that we have to overcome is that to a first approximation the oscillatory bulk flow merely carries the concentration back and forth at velocity $\bar{u}_\mu$ without any net dispersion. In the absence of branching (Smith 1977), we can suppress these rapid oscillations in concentration by using a volume-following coordinate.

On the flood tide (inhalation) the tracer distribution gets split up at every branching. Then on the ebb tide (exhalation) the different parts of the tracer distribution come together and mix. A possible dispersion mechanism (Schijf & Schonfeld 1953) is that there could be non-synchronous ventilation such that the moving coordinates in the different branches get displaced from each other depending upon the phase differences between the flows. Here we shall exclude that dispersion mechanism by assuming that at leading order there is perfect synchronism of the flow in the merging branches. The fraction of the oscillatory volume flux $A_\mu u_\mu^{(0)}$ entering or leaving each branch is assumed to be proportional to the volume upstream of that branch. No matter which splitting is followed, the volume-following time-cycle average of the frame velocity is zero, $\langle u_{\mu'}^{(0)} \rangle = 0$. The angle brackets $\langle \ldots \rangle$ denote time averaging.

Within the single outermost channel, we use the volume to define a volume-following coordinate:

$$\xi = V(x,t)\,. \tag{4.1}$$

The assumption about the division of the oscillatory flow between the branches requires us to use a stretched volume coordinate in tributaries (bigger stretching for smaller interior volumes):

$$\xi = P_\mu V_\mu(x,t)\,, \quad \text{with} \quad P_{\mu_N} = \prod_{j=1}^{N} \frac{V_{\mu_{j-1}}(x^-_{\mu_{j-1}},t)}{V_{\mu_j}(x^+_{\mu_j},t)} \tag{4.2a,b}$$

The inner ends of all channels are at $\xi = 0$. Unlike the interior volumes V_μ, the coordinate ξ has been constructed to be continuous across junctions. The synchronism assumption implies that P_μ is independent of time t and that at the merger of two or more channels, the product $P_\mu A_\mu u_\mu^{(0)}$ has the same value in all of those channels.

For the example of an infinite geometric series used at the end of §2, all the branches at a particular generation are identical and the ξ-construction is almost trivial. The individual quotients in the product (4.2*b*) all have the value M, so we have $P_{\mu_N} = M^N$. Within each of the M^N members of the Nth generation, with $\Lambda^{N+1}L \leqslant x \leqslant \Lambda^N L$, the formula for the volume-following coordinate becomes

$$\xi = (M\alpha\Lambda)^{N+1}\frac{(1-\Lambda)LA}{(1-M\alpha\Lambda)} + (M\alpha)^N(x - L\Lambda^{N+1})A \quad . \tag{4.3}$$

Figure 2 shows the piecewise linear relationship between the volume-following coordinate ξ and the conventional longitudinal coordinate x in the special case $\Lambda = 0.5$, $M = 2$. Small dots indicate the positions of junctions. If the flood tide (inhalation) is modelled by increasing α, then the fluid at a fixed ξ-value is drawn inwards to a smaller x-location. On the ebb (exhalation) α decreases back to the original value and the fluid again moves outward to a larger x-location. The to-and-fro movement at velocity $u_{\mu'}^{(0)}$, may involve crossing several junctions, particularly for large α with small ξ/LA.

To avoid spurious calculations outside the mouth, we specify low tide (minimum lung volume) t_{low} as the reference time. At that time, a given ξ-value and given multi-index selection of channels $\boldsymbol{\mu}$ define a unique channel. The connectivity at t_{low} determines how the concentration and concentration flux in different branches of the network should be matched. At another time the fluid will have retreated further from the mouth. If ξ is closer than an excursion distance from a junction, then the

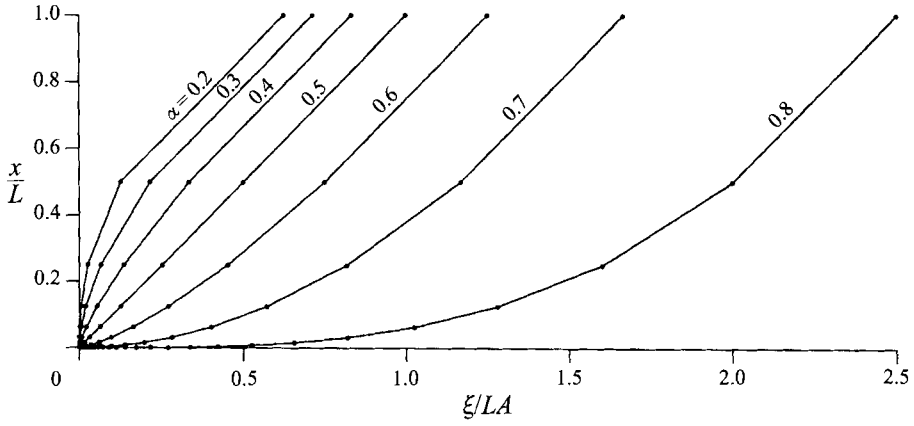

FIGURE 2. Longitudinal position as a function of the volume-following coordinate ξ along bifurcating channels ($M = 2$) with fixed length ratio $A = 0.5$ but varying area ratios α.

initial selection of channels μ will have become split into several μ' channels. To accommodate this oscillatory splitting, we introduce an area-weighted cycle average, denoted with a tilde, involving a summation restricted to those μ' channels:

$$\tilde{c}_\mu \left\langle \sum_{\mu'} A_{\mu'} \right\rangle = \left\langle \sum_{\mu'} A_{\mu'} \bar{c}_{\mu'} \right\rangle . \tag{4.4}$$

In the volume-following frame of reference, the equation for the concentration can be written

$$m_1 m_2 m_3 \left(\partial_t c + (u - \bar{u}_{\mu'}) P_{\mu'} A_{\mu'} \partial_\xi c + v \partial_y c + w \partial_z c\right) + \varepsilon P_{\mu'} Q_{\mu'} \partial_\xi c$$
$$- P_{\mu'} A_{\mu'} \partial_\xi \left(\frac{m_2 m_3}{m_1} \kappa_1 P_{\mu'} A_{\mu'} \partial_\xi c \right) - \partial_y \left(\frac{m_1 m_3}{m_2} \kappa_2 \partial_y c \right) - \partial_z \left(\frac{m_1 m_2}{m_3} \kappa_3 \partial_z c \right) = 0. \tag{4.5}$$

The μ' subscripts emphasize that in the moving frame, as the flow retreats/advances and the channels split/merge, the values of certain coefficients can jump in value. However, as ξ varies across junctions, the concentration $c(\xi, y, z, t)$ must remain continuous.

5. Volumetric centroid displacement

By construction, the time-dependent distortions and splitting of the flow geometry in the volume-following ξ frame of reference eliminates the most rapid time-dependence of the concentration. To account for the relative narrowness of the channels and for the slow time evolution of $\tilde{c}$, we introduce a longer length scale χ and a second time scale:

$$\chi = \varepsilon \xi , \quad \tau = \varepsilon^2 t . \tag{5.1}$$

Paying careful attention to there being two co-existing time coordinates t and τ we can re-write the advection-diffusion equation (4.5) in an extended and scaled form:

$$m_1m_2m_3(\partial_t c + v\partial_y c + w\partial_z c) - \partial_y\left(\frac{m_1m_3}{m_2}\kappa_2\partial_y c\right) - \partial_z\left(\frac{m_1m_2}{m_3}\kappa_3\partial_z c\right)$$
$$= -\varepsilon m_1m_2m_3(u-\bar{u}_{\mu'})P_{\mu'}A_{\mu'}\frac{\partial c}{\partial\chi} - \varepsilon^2 m_1m_2m_3\frac{\partial c}{\partial\tau}$$
$$-\varepsilon^2 m_1m_2m_3P_{\mu'}Q_{\mu'}\frac{\partial c}{\partial\chi} + \varepsilon^2 P_{\mu'}A_{\mu'}\frac{\partial}{\partial\chi}\left(\frac{m_2m_3}{m_1}\kappa_1 P_{\mu'}A_{\mu'}\frac{\partial c}{\partial\chi}\right) \tag{5.2}$$

In the spirit of the work of Taylor (1953), we assume that sufficient time has elapsed that the concentration varies slowly with respect to the short length and time scales (y,z,t) and departs only by order ε from the volume-following, area-weighted cycle average $\tilde{c}$. We can regard the residual concentration fluctuations across the flow as being forced by the right-hand-side terms in (5.2):

$$c = \tilde{c} - \varepsilon G(\chi,y,z,t)\frac{\partial\tilde{c}}{\partial\chi} + \varepsilon^2 c_2 + \dots\ , \tag{5.3}$$

with

$$m_1m_2m_3(\partial_t G + v\partial_y G + w\partial_z G) - \partial_y\left(\frac{m_1m_3}{m_2}\kappa_2\partial_y G\right) - \partial_z\left(\frac{m_1m_2}{m_3}\kappa_3\partial_z G\right)$$
$$= m_1m_2m_3(u-\bar{u}_{\mu'})P_{\mu'}A_{\mu'}\ . \tag{5.4}$$

The volumetric centroid displacement or distortion function G accommodates the gradual tendency for the concentration distribution to become displaced outward (or inwards) where the outward flow is greater (or less) than the cross-sectional average outflow. At each tributary (alveolus) feeding the system we require that G is initially zero. As χ varies, the splitting of the geometry in the moving frame of reference occurs at slightly different times. Importantly, $G(\chi,y,z,t)$ remains continuous. Integrating equation (5.4) across a sub-channel, allows us to show that $A_\mu\bar{G}_\mu$ is zero along the innermost channels and constant along subsequent channels. It is possible that in individual sub-channels $\bar{G}_\mu \neq 0$. However, the continuity of G across junctions allows us to conclude that the weighted sum $\tilde{G}_\mu$ is zero. The synchronism assumption requires that when the topology splits $P_{\mu'}A_{\mu'}\bar{u}_{\mu'}$ is the same for all sub-channels and for the merged channel. Thus, the right-hand-side forcing term in equation (5.4) adjusts more in shape than in size.

If we multiply both sides of (5.4) by $G(\chi,y,z,t)$, and integrate across a sub-channel, then we can derive the identity

$$P_{\mu'}A_{\mu'}\int_{\Omega_{\mu'}}(u-\bar{u}_{\mu'})G\mathrm{d}\Omega = \frac{1}{2}\frac{\partial}{\partial t}\int_{\Omega_{\mu'}}G^2\mathrm{d}\Omega + \int_{\Omega_{\mu'}}\left\{\kappa_2\left(\frac{\partial_y G}{m_2}\right)^2 + \kappa_3\left(\frac{\partial_z G}{m_3}\right)^2\right\}\mathrm{d}\Omega\ . \tag{5.5}$$

We use the final integral to define a quantity $S_{\mu'}$, with units L^6/T, which is identified in the next section as being the volumetric shear dispersion coefficient:

$$S_{\mu'} = \frac{1}{A_{\mu'}}\int_{\Omega_{\mu'}}\left\{\kappa_2\left(\frac{\partial_y G}{m_2}\right)^2 + \kappa_3\left(\frac{\partial_z G}{m_3}\right)^2\right\}\mathrm{d}\Omega\ . \tag{5.6}$$

Any geometrical or flow property, such as splitting, that increases the gradients of the volumetric centroid displacement function G necessarily increases the shear dispersion.

6. Shear dispersion equation

Integrating the order-ε^2 terms in (5.2) over the sum of all the sub-channels, using the identity (5.5) then taking volume-following cycle average, we obtain an advection-diffusion equation:

$$\left\langle \sum_{\mu'} A_{\mu'} \right\rangle \frac{\partial \tilde{c}}{\partial \tau} + \left\{ \left\langle \sum_{\mu'} P_{\mu'} A_{\mu'} Q_{\mu'} \right\rangle + \left\langle \sum_{\mu'} P_{\mu'}^2 A_{\mu'}^2 \overline{\left(\frac{\kappa_1}{m_1^2}\right)} \frac{\partial A_{\mu'}}{\partial \chi} \right\rangle \right\} \frac{\partial \tilde{c}}{\partial \chi}$$
$$- \frac{\partial}{\partial \chi} \left(\left\{ \left\langle \sum_{\mu'} P_{\mu'}^2 A_{\mu'}^3 \overline{\left(\frac{\kappa_1}{m_1^2}\right)} \right\rangle + \left\langle \sum_{\mu'} A_{\mu'} S_{\mu'} \right\rangle \right\} \frac{\partial \tilde{c}}{\partial \chi} \right) = 0 . \quad (6.1)$$

It is this equation that identifies $\tilde{S}_\mu$ as being the cycle-averaged volumetric shear dispersion coefficient. In the unscaled (ξ, t) coordinates the mean flow $Q_{\mu'}$ term recovers its ε multiplier:

$$\left\langle \sum_{\mu'} A_{\mu'} \right\rangle \frac{\partial \tilde{c}}{\partial t} + \left\{ \left\langle \sum_{\mu'} P_{\mu'} A_{\mu'} \varepsilon Q_{\mu'} \right\rangle + \left\langle \sum_{\mu'} P_{\mu'}^2 A_{\mu'}^2 \overline{\left(\frac{\kappa_1}{m_1^2}\right)} \frac{\partial A_{\mu'}}{\partial \xi} \right\rangle \right\} \frac{\partial \tilde{c}}{\partial \xi}$$
$$- \frac{\partial}{\partial \xi} \left(\left\{ \left\langle \sum_{\mu'} P_{\mu'}^2 A_{\mu'}^3 \overline{\left(\frac{\kappa_1}{m_1^2}\right)} \right\rangle + \left\langle \sum_{\mu'} A_{\mu'} S_{\mu'} \right\rangle \right\} \frac{\partial \tilde{c}}{\partial \xi} \right) = 0 . \quad (6.2)$$

It is conventional to quantify the centroid displacement in terms of a longitudinal distance and the effects of shear as an augmented longitudinal diffusivity (Taylor 1953). By analogy with the discontinuous interior volumes V_μ, we use the t_{low} cross-sectional area $A_\mu(\overline{m_1^{-1}})_\mu$ and the associated product P_μ to define a discontinuous local centroid displacement (distance) function:

$$g_\mu(\chi, y, z, t) = \frac{G(\chi, y, z, t)}{P_\mu A_\mu (\overline{m_1^{-1}})_\mu} . \quad (6.3)$$

The corresponding local instantaneous shear dispersion coefficient for an individual channel cross-section is

$$D_{\mu'} = \left(\frac{P_\mu A_\mu}{P_{\mu'} A_{\mu'}}\right)^2 \frac{1}{A_{\mu'}} \int_{\Omega_{\mu'}} \left\{ \kappa_2 \left(\frac{\partial_y g_\mu}{m_2}\right)^2 + \kappa_3 \left(\frac{\partial_z g_\mu}{m_3}\right)^2 \right\} d\Omega . \quad (6.4)$$

The shear dispersion term on the right-hand side of (6.2) can then be written

$$\frac{\partial}{\partial \xi} \left(\left\langle \sum_{\mu'} P_{\mu'}^2 A_{\mu'}^3 D_{\mu'} \right\rangle \left(\overline{m_1^{-1}}\right)_\mu^2 \frac{\partial \tilde{c}}{\partial \xi} \right) . \quad (6.5)$$

A factor $(P_{\mu'} A_{\mu'} (\overline{m_1^{-1}})_{\mu'})^2$ converts the distance measure $D_{\mu'}$ of dispersion, with units L^2/T, to the volumetric measure $S_{\mu'}$. If as in lungs the total area increases away from the mouth, then by mass conservation the velocities $\bar{u}_{\mu'}$ decrease and the products $P_{\mu'} A_{\mu'}$ increase. Hence the reduction in $D_{\mu'}$ away from the mouth is much more severe than the reduction in $\tilde{S}_\mu$. For example, Paloski *et al.* (1987) conducted experiments with branching identical Y-tubes. In their figure 4, the reduction in $D_{\mu'}$ at each generation away from the mouth corresponds approximately to the factor of 4 jump in $(P_{\mu'} A_{\mu'})^2$. Thus, for their experiments , $\tilde{S}_\mu$ does not vary markedly. Of course, the relative increase in dispersion by comparison to non-branching channels, by up to a

factor of 3 as found by Paloski *et al.* (1987), is the same whichever measure $D_{\mu'}$ or $\widetilde{S}_{\mu}$ is used.

Since the junction locations in the volume-following coordinates (ξ, t) are inherited from the geometry at low tide (minimum lung volume), we can use the x-coordinate and volume derivatives A_{μ} at that reference time t_{low} to determine an (x, t) counterpart to equation (6.2):

$$0 = \left\langle \sum_{\mu'} A_{\mu'} \right\rangle \frac{\partial \widetilde{c}}{\partial t} + \left\{ \left\langle \sum_{\mu'} \frac{P_{\mu'} A_{\mu'}}{P_{\mu} A_{\mu}} Q_{\mu'} \right\rangle + \left\langle \sum_{\mu'} \frac{P_{\mu'} A_{\mu'}^2}{P_{\mu} A_{\mu}^2} \overline{\left(\frac{\kappa_1}{m_1^2} \right)} \frac{\partial A_{\mu'}}{\partial x} \right\rangle \right\} \frac{\partial \widetilde{c}}{\partial x}$$
$$- \frac{1}{A_{\mu}} \frac{\partial}{\partial x} \left(\left\{ \left\langle \sum_{\mu'} \frac{P_{\mu'}^2 A_{\mu'}^3}{P_{\mu}^2 A_{\mu}^2} \overline{\left(\frac{\kappa_1}{m_1^2} \right)} \right\rangle + \left\langle \sum_{\mu'} \frac{P_{\mu'}^2 A_{\mu'}^3}{P_{\mu}^2 A_{\mu}^2} D_{\mu'} \right\rangle \left(\overline{m_1^{-1}} \right)_{\mu}^2 \right\} \frac{\partial \widetilde{c}}{\partial x} \right) . \qquad (6.6)$$

This formulation (6.6) of the shear dispersion equation can be interpreted as a flow-splitting, volume-following, time-cycle-averaged version of (3.6). The μ' terms are periodic and the μ terms are t_{low} values. For a single channel with rapid mixing Shinohara *et al.* (1969) and Smith (1977) could justify dividing through by the area $A_{\mu'}$ prior to taking the cycle average. Thus, they obtained quadratic $A_{\mu'}^2$ rather than cubic $A_{\mu'}^3$ weighting for the effective long-term dispersion coefficient and other minor departures from (6.6).

In (6.2) or (6.6), the river volume fluxes $Q_{\mu'}$ (net gas volume fluxes across the alveoli) result in an outward drift. The $P_{\mu'} A_{\mu'}$-weighting emphasizes the volume fluxes into channels with low oscillatory velocity. The awkward form of the longitudinal diffusion terms is a consequence of the local shortening in regions of locally large cross-sectional area and the abrupt change in length scale for longitudinal concentration gradients (and changed numbers of channels) every time a junction is crossed. Outward increases in area ($\partial A_{\mu'}/\partial x > 0$) result in augmented outward diffusive transport, which takes the form of an apparent outward drift velocity in (6.2) or (6.6).

At the low-tide (minimum lung volume) position of junctions, the change in numbers of channels involved in the μ' summations necessarily implies jumps in the coefficients in equation (6.2) or (6.6). Across junctions there has to be matching of the cycle-averaged concentration $\widetilde{c}$ and matching of the sum over the merging branches of the fluxes:

$$\left\{ \left\langle \sum_{\mu'} P_{\mu'} A_{\mu'} \varepsilon Q_{\mu'} \right\rangle + \left\langle \sum_{\mu'} P_{\mu'}^2 A_{\mu'}^2 \overline{\left(\frac{\kappa_1}{m_1^2} \right)} \frac{\partial A_{\mu'}}{\partial \xi} \right\rangle \right\} \widetilde{c}$$
$$- \left\{ \left\langle \sum_{\mu'} P_{\mu'}^2 A_{\mu'}^3 \overline{\left(\frac{\kappa_1}{m_1^2} \right)} \right\rangle + \left\langle \sum_{\mu'} A_{\mu'} S_{\mu'} \right\rangle \right\} \frac{\partial \widetilde{c}}{\partial \xi} , \qquad (6.7)$$

with the corresponding flux in the merged channel. At each tributary (alveolus) feeding the system and at the mouth, typical end conditions would be imposed values for the cycle-averaged fluxes or for the cycle-averaged concentration $\widetilde{c} = b_{\mu}(t)$.

7. Modes for self-similar channels with weak cross-flow

The complexity of (5.4) for the volumetric centroid displacement, with time-dependent splitting and re-joining, is a formidable obstacle to the implementation of the advection-diffusion equation (6.6). In this section we simplify the equation, geometry and transverse diffusion to achieve a formal series solution.

As a first simplification, we assume that in (5.4), the cross-flow (v, w) is dominated by diffusion $(\kappa_2\partial_y, \kappa_3\partial_z)$:

$$m_1m_2m_3\partial_t G - \partial_y\left(\frac{m_1m_3}{m_2}\kappa_2\partial_y G\right) - \partial_z\left(\frac{m_1m_2}{m_3}\kappa_3\partial_z G\right) = m_1m_2m_3(u-\bar{u}_{\mu'})P_{\mu'}A_{\mu'} \ . \quad (7.1)$$

In the (y,z)-plane the normal component of the flux $(-\kappa_2\partial_y G/m_2, -\kappa_3\partial_z G/m_3)$ is zero on lateral boundaries. When the flow geometry in the moving frame of reference splits up or re-connects, G must remain continuous (following the particles if there is a short velocity adjustment region). Pedley & Kamm (1988) have investigated the opposite limit of strong secondary flows, but not the effect of splitting.

As a second simplification we assume that between splitting and re-joining events the geometry is self-similar, with changes in scale accommodated via the metric coefficients m_2, m_3. If in addition, the transverse diffusivities κ_2, κ_3 are self-similar, then it is convenient to introduce a set of eigenmodes $\{\psi^{(k)}_{\mu'}(y,z)\}$ corresponding to separation of variables with respect to the longitudinal coordinate:

$$\partial_y\left(\frac{m_1m_3}{m_2}\kappa_2\partial_y\psi^{(k)}_{\mu'}\right) + \partial_z\left(\frac{m_1m_2}{m_3}\kappa_3\partial_z\psi^{(k)}_{\mu'}\right) + \lambda^{(k)}_{\mu'}m_1m_2m_3\psi^{(k)}_{\mu'} = 0 \quad (7.2a)$$

with

$$\overline{(\psi^{(k)}_{\mu'})^2} = 1 \ , \quad \overline{\kappa_2\left(\frac{\partial_y\psi^{(k)}_{\mu'}}{m_2}\right)^2} + \overline{\kappa_3\left(\frac{\partial_z\psi^{(k)}_{\mu'}}{m_3}\right)^2} = \lambda^{(k)}_{\mu'}, \quad (7.2b,c)$$

$$\psi^{(0)}_{\mu'} = 1 \ , \quad \lambda^{(0)}_{\mu'} = 0 \ , \quad \text{and} \quad \lambda^{(1)}_{\mu'}(\xi,t) < \lambda^{(2)}_{\mu'}(\xi,t) < \ldots \quad (7.2d,e,f)$$

The eigenvalues $\{\lambda^{(k)}_{\mu'}\}$ will be systematically larger in the narrower channels further from the mouth. If the same similarity extends to other sub-channels, then a suitable shift of (y,z) coordinates will allow us to use the same eigenmodes $\psi^{(k)}$ and the μ' subscripts can be suppressed.

For circular cylindrical tubes of radius a with isotropic diffusivity κ and symmetry about $\theta = 0$, the non-constant modes involve Bessel functions. It is not until $k = 3$ that an axisymmetric mode arises:

$$\psi^{(1)} = \frac{j'_{1,1}}{(j'^{\,2}_{1,1}-1)^{1/2}}\cos(\theta)\frac{J_1(j'_{1,1}y)}{J_1(j'_{1,1})} \ , \ \lambda^{(1)}_{\mu'} = \frac{\kappa}{a^2}j'^{\,2}_{1,1} \ , \ j'_{1,1} = 1.84118 \ , \quad (7.3a,b,c)$$

$$\psi^{(2)} = \frac{j'_{2,1}}{(j'^{\,2}_{2,1}-4)^{1/2}}\cos(2\theta)\frac{J_2(j'_{2,1}y)}{J_2(j'_{2,1})} \ , \ \lambda^{(2)}_{\mu'} = \frac{\kappa}{a^2}j'^{\,2}_{2,1} \ , \ j'_{2,1} = 3.05424 \ , \quad (7.3d,e,f)$$

$$\psi^{(3)} = \frac{J_0(j'_{0,2}y)}{J_0(j'_{0,2})} \ , \ \lambda^{(3)}_{\mu'} = \frac{\kappa}{a^2}j'^{\,2}_{0,2} \ , \ j'_{0,2} = 3.83170 \ . \quad (7.3g,h,i)$$

Thus, non-axisymmetric concentration perturbations induced at branching are remarkably long lasting. Such asymmetric modes can contribute significantly to the shear dispersion, even if the velocity profiles are symmetric.

Within the μ' sub-channel, we can represent the shear, volumetric centroid displacement function and volumetric shear dispersion in terms of the modes

$$u = \bar{u}_{\mu'} + \sum_{k=1}^{\infty} u_{\mu'}^{(k)}(\xi,t)\psi_{\mu'}^{(k)}(y,z) \ , \quad u_{\mu'}^{(k)}(\xi,t) = \overline{(u-\bar{u}_{\mu'})\psi_{\mu'}^{(k)}} \ , \tag{7.4a,b}$$

$$G_{\mu'} = \bar{G}_{\mu'} + \sum_{k=1}^{\infty} G_{\mu'}^{(k)}(\xi,t)\psi_{\mu'}^{(k)}(y,z) \ , \quad S_{\mu'} = \sum_{k=1}^{\infty} G_{\mu'}^{(k)}(\xi,t)^2 \lambda_{\mu'}^{(k)} \ . \tag{7.4c,d}$$

$\bar{G}_{\mu'}$ does not contribute to the shear dispersion, does not interact with the other modes (when summed over all the sub-channels) and does not need to be calculated.

The three-dimensional second-order partial differential equation (7.1) is replaced by a series of two-dimensional first-order equations:

$$\partial_t \bar{G}_{\mu'} = 0 \ , \quad \partial_t G_{\mu'}^{(k)} + \lambda_{\mu'}^{(k)} G_{\mu'}^{(k)} = u_{\mu'}^{(k)}(\xi,t) P_{\mu'} A_{\mu'} \ . \tag{7.5a,b}$$

For the high-order modes or narrow channels with large $\lambda_{\mu'}^{(k)}$, we can estimate that

$$G_{\mu'}^{(k)} \sim P_{\mu'} A_{\mu'} \frac{u_{\mu'}^{(k)}}{\lambda_{\mu'}^{(k)}} \ . \tag{7.6}$$

Thus, S_μ and the related shear dispersion tend to be dominated by the first few modes.

If for a given low-tide (minimum lung volume) position ξ in the μ channel the volume-following geometry does not divide, then $\bar{G}_\mu$ remains zero and the solutions for the higher amplitudes can be written

$$G_\mu^{(k)}(\xi,t) = P_\mu \int_{-\infty}^{t} A_\mu(\xi,t') u_\mu^{(k)}(\xi,t') \exp\left\{ -\int_{t'}^{t} \lambda_\mu^{(k)}(\xi,t'')\mathrm{d}t'' \right\} \mathrm{d}t' . \tag{7.7}$$

It is only modes with non-zero velocity forcing $u_\mu^{(k)}$ that contribute to the centroid displacement or to the shear dispersion (7.4*d*). For example, axisymmetric flows in non-branching cylindrical tubes only involve axisymmetric modes.

If the attenuation rates $\lambda_\mu^{(k)}$ and the volume derivatives A_μ are constant and if the self-similar flow is sinusoidal, then the non-branching result (7.7) yields a time-lagged sinusoidal result for the volumetric centroid displacement:

$$u_\mu^{(k)} = U_\mu^{(k)} \sin(\omega t) \ , \quad G_\mu^{(k)} = f_\mu^{(k)}(t) \equiv P_\mu A_\mu U_\mu^{(k)} \frac{\lambda_\mu^{(k)} \sin(\omega t) - \omega \cos(\omega t)}{(\lambda_\mu^{(k)})^2 + \omega^2} \ , \tag{7.8a,b}$$

$$\left(\overline{m_1^{-1}}\right)_\mu^2 \langle D_\mu \rangle = \frac{1}{2} \sum_{k=1}^{\infty} \frac{U_\mu^{(k)2} \lambda_\mu^{(k)}}{(\lambda_\mu^{(k)})^2 + \omega^2} \ , \quad \widetilde{S}_\mu(\omega,\infty) = \frac{1}{2} \sum_{k=1}^{\infty} \frac{(P_\mu A_\mu U_\mu^{(k)})^2 \lambda_\mu^{(k)}}{(\lambda_\mu^{(k)})^2 + \omega^2} \ . \tag{7.8c,d}$$

For low frequencies $\omega < \lambda_\mu^{(k)}$, the centroid displacement component $G_\mu^{(k)}$ is in phase with the current. Later in this paper the branching solution for $G_\mu^{(k)}$ will be written as a perturbation from the solution (7.8*b*). In (7.8*c,d*), the denominator quantifies the effect of rapid flow oscillations (large ω) in reducing the shear dispersion (Chatwin 1975; Watson 1983). Since $P_\mu A_\mu \bar{u}_\mu$ is the same in sub-channels as in the main channel, the between-channel changes in the reference values $\widetilde{S}_\mu(\omega,\infty)$ are linked to changes in the decay rates $\lambda_\mu^{(k)}$. In the present context, the symbol ∞ signifies more than an excursion distance from junctions, i.e unaffected by branching.

8. Allowing for branching in the modal solution

For a particular low-tide (minimum lung volume) position ξ in the μ channel we denote the volume-following splitting times on flood tide (inhalation) by $t_{\mu}^{-}(\xi)$, $t_{\mu'}^{-}(\xi)$. The corresponding re-connection times on ebb tide (exhalation) are denoted $t_{\mu'}^{+}(\xi)$, $t_{\mu}^{+}(\xi)$. If the adjustment of geometry and velocity across junctions takes place rapidly relative to cross-channel mixing, then at the transition times we can use the particle-following matching (Daish 1985):

$$G_{\mu',i}^{(l)}(x_{\mu',i}{}^{+},\ t) = \sum_{k=1}^{\infty} F_{\mu',i}^{(k,l)}(t) G_{\mu'}^{(k)}(x_{\mu'}{}^{-},\ t) \quad \text{used on flood (inhalation)}\ , \tag{8.1a}$$

$$G_{\mu'}^{(k)}(x_{\mu'}{}^{-},\ t) = \sum_{i=1}^{M} \sum_{l=1}^{\infty} E_{\mu',i}^{(k,l)}(t) G_{\mu',i}^{(l)}(x_{\mu',i}{}^{+},\ t) \quad \text{used on ebb (exhalation)}\ , \tag{8.1b}$$

with

$$\delta_{km} = \sum_{i=1}^{M} \sum_{l=1}^{\infty} E_{\mu',i}^{(k,l)} F_{\mu',i}^{(m,l)}\ . \tag{8.1c}$$

The flood and ebb coefficients $F_{\mu',i}^{(k,l)}(t)$ and $E_{\mu',i}^{(k,l)}(t)$ involve integrals of products of $\psi_{\mu'}^{(k)}$ for the outer channel and $\psi_{\mu',i}^{(l)}$ for the inner sub-channel, with particle-following matching of cross-stream positions (3.5):

$$F_{\mu',i}^{(k,l)} = \frac{1}{A_{\mu',i}} \int_{\Omega_{\mu',i}} \psi_{\mu'}^{(k)}(Y_{\mu',i}^{+},\ Z_{\mu',i}^{+}) \psi_{\mu',i}^{(l)}(y,z)\mathrm{d}\Omega\ , \tag{8.2a}$$

$$E_{\mu',i}^{(k,l)} = \frac{1}{A_{\mu'}} \int_{\Omega_{\mu'}} \psi_{\mu'}^{(k)}(y,z) \psi_{\mu',i}^{(l)}(Y_{\mu',i}^{-},\ Z_{\mu',i}^{-})\mathrm{d}\Omega\ . \tag{8.2b}$$

Outside the range of $(Y_{\mu',i}^{-},\ Z_{\mu',i}^{-})$ the function $\psi_{\mu',i}^{(l)}$ is extended by zero (i.e. where the fluid does not come from the μ', i sub-channel). Self-similarity of the velocity profile implies that $F_{\mu',i}^{(k,l)}$ and $E_{\mu',i}^{(k,l)}$ are independent of time.

Figures 3 and 4 show the first few flood and ebb coefficients, as calculated in § 12, for a sub-channel $\mu, 1$ which exchanges a fraction $(1+\phi)/2$ of the oscillatory volume flux from a similarly shaped channel μ. In the limit as ϕ tends to -1 the sub-channel is vanishingly small and the matching coefficients are all zero. Conversely, as ϕ tends to 1, the sub-channel is indistinguishable from the merged channel so the diagonal coefficients $F_{\mu,i}^{(k,k)}$, $E_{\mu,i}^{(k,k)}$ tend to 1 while the off-diagonal terms tend to zero.

On flood tide (inhalation) the matching (8.1a) gives the starting values at time $t_{\mu'}^{-}(\xi)$ for the amplitudes of the modes in the μ', i sub-channel. Until a further splitting or subsequent re-connection, the volume-following solution for a given value of ξ can be written

$$\begin{aligned} G_{\mu',i}^{(l)}(t) = {} & \exp\left\{ -\int_{t_{\mu'}^{-}}^{t} \lambda_{\mu',i}^{(l)}(t')\mathrm{d}t' \right\} G_{\mu',i}^{(l)}(t_{\mu'}^{-}) \\ & + P_{\mu',i} \int_{t_{\mu'}^{-}}^{t} A_{\mu',i}(t') u_{\mu',i}^{(l)}(t') \exp\left\{ -\int_{t'}^{t} \lambda_{\mu',i}^{(l)}(t'')\mathrm{d}t'' \right\} \mathrm{d}t'\ . \end{aligned} \tag{8.3}$$

At time $t_{\mu'}^{+}(\xi)$ on ebb tide (exhalation) when the μ', i sub-channels reconnect to form

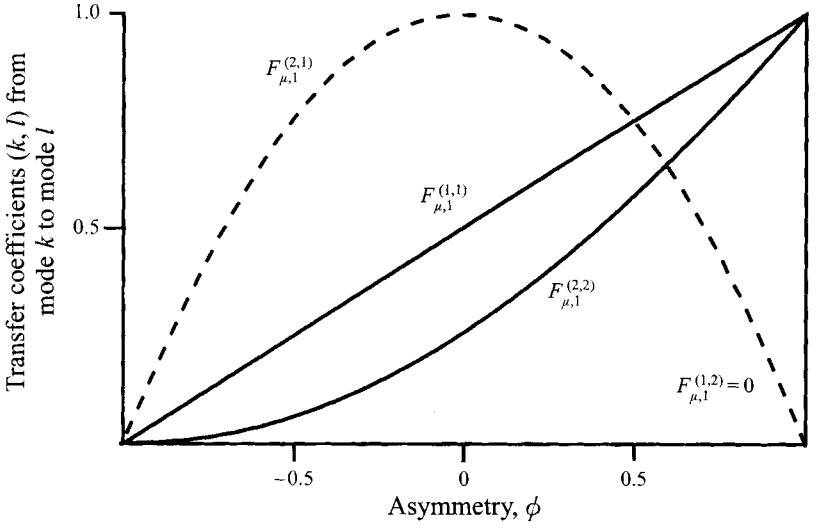

FIGURE 3. Flood (inhalation) matching coefficients as a function of the asymmetry.

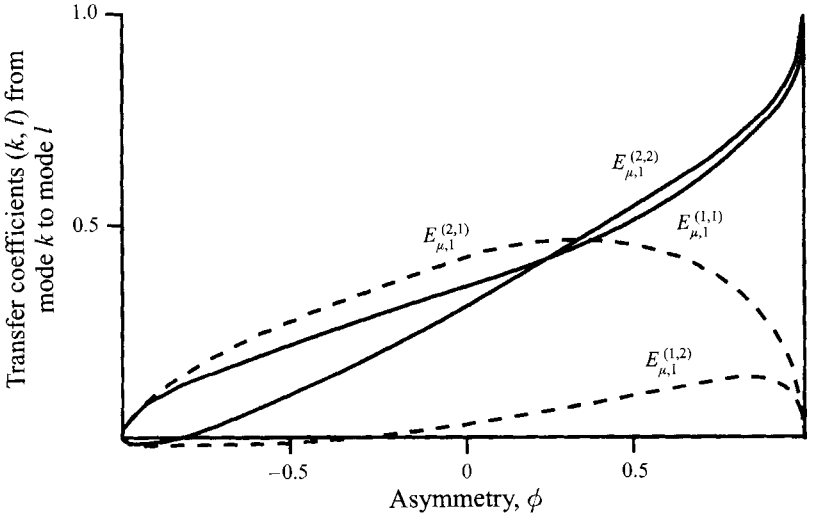

FIGURE 4. Ebb (exhalation) matching coefficients as a function of the asymmetry.

a μ' channel, it is the matching (8.1*b*) that provides the starting values:

$$G^{(k)}_{\mu'}(t) = \exp\left\{-\int_{t^+_{\mu'}}^{t} \lambda^{(k)}_{\mu',i}(t')\mathrm{d}t'\right\} G^{(k)}_{\mu'}(t^+_{\mu'}) + P_{\mu'}\int_{t^+_{\mu}}^{t} A_{\mu'}(t')u^{(k)}_{\mu'}(t')\exp\left\{-\int_{t'}^{t}\lambda^{(k)}_{\mu'}(t'')\mathrm{d}t''\right\}\mathrm{d}t' \,. \tag{8.4}$$

For high-order modes or narrow channels with $\lambda^{(k)}_{\mu'}$ larger than the frequency of oscillations, there is exponentially fast approach to the non-branching result (7.7). When there is branching, the splitting and merging $F^{(k,l)}_{\mu',i}$ and $E^{(k,l)}_{\mu',i}$ terms in the formulae (8.1*a*,*b*) for $G^{(l)}_{\mu',i}(t^-_{\mu'})$, $G^{(k)}_{\mu'}(t^+_{\mu'})$ allow there to be contributions to the volumetric

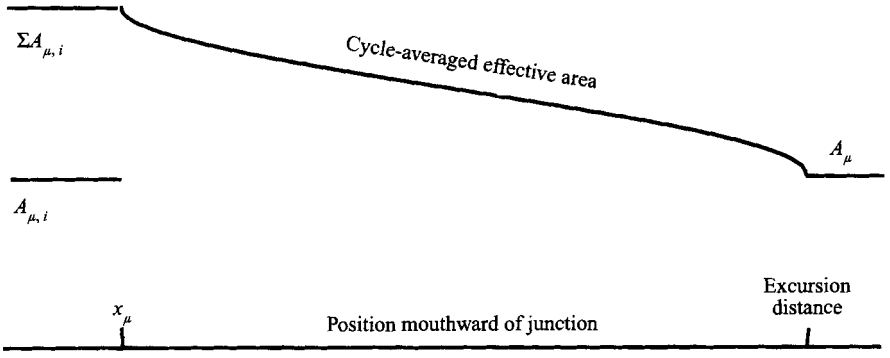

FIGURE 5. Cycle-averaged effective area across the low-tide location of a junction.

centroid displacement from modes with $u^{(l)}_{\mu',i}$ or $u^{(k)}_{\mu'}$ identically zero. In particular, for cylindrical tubes with axisymmetric velocity profiles, the relatively long-lasting non-symmetric modes (7.3*a*,*d*) can be induced at branching.

For steady flows with junctions Saffman (1969), Ultman & Blatman (1977), and Adler (1985), made the assumption that at every junction there is vigorous and complete mixing. This corresponds to setting $G^{(l)}_{\mu',i}(t^-_{\mu'})$, $G^{(k)}_{\mu'}(t^+_{\mu'})$ equal to zero in the above equations (8.3), (8.4) or equivalently, to setting $F^{(k,l)}_{\mu',i}$, $E^{(k,l)}_{\mu',i}$ equal to zero.

9. Sinusoidal flows along piecewise-uniform channels

We assume that the cross-sectionally averaged flow is sinusoidal:

$$\bar{u} = -\hat{U}\sin(\omega t)\,,\quad x(\xi,t) = x(\xi,0) - \frac{\hat{U}}{\omega}[1-\cos(\omega t)]\,. \tag{9.1a,b}$$

The tidal phase $\Theta_\mu = \omega t^-_\mu$ of the first splitting on the flood (inhalation) increases from 0 to π as the low-tide (minimum lung volume) position moves from a junction x_μ to a full excursion mouthwards $x_\mu + 2\hat{U}/\omega$:

$$\Theta_\mu = \arccos\left(1 - \frac{\omega(x-x_\mu)}{\hat{U}}\right)\,,\ \text{with return time}\quad \omega t^+_\mu = 2\pi - \Theta_\mu\,. \tag{9.2a,b}$$

The time spent in the μ channel is proportional to Θ_μ and the time spent in a μ,i sub-channel is proportional to $\Theta_{\mu,i} = \pi - \Theta_\mu$. Thus, the volume-following, cycle-averaged effective area term in (6.2) is given by

$$\left\langle \sum_{\mu'} A_{\mu'} \right\rangle = \frac{\Theta_{\mu,i}}{\pi}\sum_{i}^{M} A_{\mu,i} + \frac{\Theta_\mu}{\pi}A_\mu \quad \text{where}\quad \Theta_{\mu,i} + \Theta_\mu = \pi\,. \tag{9.3}$$

With respect to Θ_μ/π, there is a linear transition from the sum of the areas $A_{\mu,i}$ of the sub-channels to the area A_μ of the merged channel. Figure 5 shows the effective area as the low-tide (fully exhaled) position x moves outward across a junction x_μ from either of two identical sub-channels to a merged channel of the same area (corresponding to the experimental configuration used by Paloski *et al.* (1987). The steepness of the graph near the junction or near an excursion limit mouthwards of the junction is a consequence of the comparatively long time as the flow turns in the main or sub-channels respectively.

For piecewise-uniform channels, with $\lambda^{(k)}_{\mu'}$ and $A_{\mu'}$ constants, the between-junction

solutions (8.3), (8.4) can be written both as a perturbation from the vigorous mixing limit and as tending towards the non-branching result (7.8*b*):

$$G^{(l)}_{\mu',i}(t) = f^{(l)}_{\mu',i}(t) + \exp\{-\lambda^{(l)}_{\mu',i}[t - t^-_{\mu'}]\}\left(\delta G^{(l)}_{\mu',i} - f^{(l)}_{\mu',i}(t^-_{\mu'})\right) , \tag{9.4a}$$

$$G^{(k)}_{\mu'}(t) = f^{(k)}_{\mu'}(t) + \exp\{-\lambda^{(k)}_{\mu'}[t - t^+_{\mu'}]\}\left(\delta G^{(k)}_{\mu'} - f^{(k)}_{\mu'}(t^+_{\mu'}))\right) . \tag{9.4b}$$

When there is just one splitting, we can use equations (9.4*a*,*b*), (8.1*a*,*b*) at successive rejoining and splitting times t^+_μ and $(2\pi/\omega + t^-_\mu)$ to derive relationships between $\delta G^{(l)}_{\mu,i}$ and $\delta G^{(k)}_\mu$ needed to guarantee periodicity:

$$\delta G^{(k)}_\mu = -\sum_{i=1}^{M}\sum_{l=1}^{\infty} E^{(k,l)}_{\mu,i}\left(\Delta^{(l)}_{\mu,i} - e^{(l)}_{\mu,i}\delta G^{(l)}_{\mu,i}\right), \tag{9.5a}$$

$$\delta G^{(l)}_{\mu,i} = \sum_{k=1}^{\infty} F^{(k,l)}_{\mu,i}\left(\Delta^{(k)}_\mu + e^{(k)}_\mu \delta G^{(k)}_\mu\right) . \tag{9.5b}$$

For compactness, we have used the notational shorthand:

$$e^{(k)}_\mu = \exp\left\{-\frac{2\lambda^{(k)}_\mu}{\omega}\Theta_\mu\right\} , \; e^{(l)}_{\mu,i} = \exp\left\{-\frac{2\lambda^{(l)}_{\mu,i}}{\omega}\Theta_{\mu,i}\right\} \text{ with } \Theta_{\mu,i} + \Theta_\mu = \pi , \tag{9.6a,b}$$

$$\Delta^{(k)}_\mu = f^{(k)}_\mu(t^-_\mu) - e^{(k)}_\mu f^{k)}_\mu(t^+_\mu) , \; \Delta^{(l)}_{\mu,i} = -f^{(l)}_{\mu,i}(t^+_\mu) + e^{(l)}_{\mu,1} f^{(l)}_{\mu,i}(t^-_\mu) . \tag{9.6c,d}$$

Hence, the exponential attenuations $e^{(k)}_\mu$ or $e^{(l)}_{\mu,i}$ respectively are close to unity and the changes in amplitudes $\Delta^{(k)}_\mu$ or $\Delta^{(l)}_{\mu,i}$ respectively are near zero, when little time is spent in the μ channel or the μ, i sub-channels. By construction $\delta G^{(k)}_\mu$ and $\delta G^{(l)}_{\mu,i}$ are zero in the limit of complete mixing at junctions. In general the linear equations (9.5) would need to be solved numerically. Conveniently, in §12 an approximate solution is given which is accurate throughout the regime in which the $\delta G^{(k)}_\mu$ and $\delta G^{(l)}_{\mu,i}$ terms contribute significantly to the volumetric shear dispersion.

When there is one splitting in the flow cycle, the volumetric shear dispersion term in (6.2) has the lengthy but explicit formula

$$\begin{aligned}
\left\langle \sum_{\mu'} A_{\mu'} S_{\mu'} \right\rangle = {} & \left(\frac{\Theta_{\mu,i}}{\pi} - \frac{\sin(2\Theta_{\mu,i})}{2\pi}\right)\sum_{i=1}^{M} A_{\mu,i}\tilde{S}_{\mu,i}(\omega,\infty) \\
& + \left(\frac{\Theta_\mu}{\pi} - \frac{\sin(2\Theta_\mu)}{2\pi}\right) A_\mu \tilde{S}_\mu(\omega,\infty) \\
& + \omega^2 \frac{\sin(2\Theta_{\mu,i})}{4\pi}\sum_{i=1}^{M} A_{\mu,i}\sum_{l=1}^{\infty}\frac{(P_{\mu,i}A_{\mu,i}U^{(l)}_{\mu,i})^2\lambda^{(l)}_{\mu,i}}{[(\lambda^{(l)}_{\mu,i})^2 + \omega^2]^2}(1 - 2e^{(l)}_{\mu,i} - e^{(l)^2}_{\mu,i}) \\
& + \omega^2 \frac{\sin(2\Theta_\mu)}{4\pi} A_\mu \sum_{k=1}^{\infty}\frac{(P_\mu A_\mu U^{(k)}_\mu)^2\lambda^{(k)}_\mu}{[(\lambda^{(k)}_\mu)^2 + \omega^2]^2}(1 - 2e^{(k)}_\mu - e^{(k)^2}_\mu) \\
& - \omega \frac{\sin(\Theta_{\mu,i})^2}{4\pi}\sum_{i=1}^{M} A_{\mu,i}\sum_{l=1}^{\infty}\frac{(P_{\mu,i}A_{\mu,i}U^{(l)}_{\mu,i})^2(\lambda^{(l)}_{\mu,i})^2}{[(\lambda^{(l)}_{\mu,i})^2 + \omega^2]^2}(3 + 4e^{(l)}_{\mu,i} + e^{(l)^2}_{\mu,i})
\end{aligned}$$

$$
\begin{aligned}
&-\omega\frac{\sin(\Theta_\mu)^2}{4\pi}A_\mu\sum_{k=1}^{\infty}\frac{(P_\mu A_\mu U_\mu^{(k)})^2(\lambda_\mu^{(k)})^2}{[(\lambda_\mu^{(k)})^2+\omega^2]^2}(3+4e_\mu^{(k)}+e_\mu^{(k)^2})\\
&+\omega^3\frac{\cos(\Theta_{\mu,i})^2}{4\pi}\sum_{i=1}^{M}A_{\mu,i}\sum_{l=1}^{\infty}\frac{(P_{\mu,i}A_{\mu,i}U_{\mu,i}^{(l)})^2}{[(\lambda_{\mu,i}^{(l)})^2+\omega^2]^2}(1-e_{\mu,i}^{(l)^2})\\
&+\omega^3\frac{\cos(\Theta_\mu)^2}{4\pi}A_\mu\sum_{k=1}^{\infty}\frac{(P_\mu A_\mu U_\mu^{(k)})^2}{[(\lambda_\mu^{(k)})^2+\omega^2]^2}(1-e_\mu^{(k)^2})\\
&+\omega\frac{\sin(\Theta_{\mu,i})}{2\pi}\sum_{i=1}^{M}A_{\mu,i}\sum_{l=1}^{\infty}\frac{P_{\mu,i}A_{\mu,i}U_{\mu,i}^{(l)}\delta G_{\mu,i}^{(l)}\lambda_{\mu,i}^{(l)}}{(\lambda_{\mu,i}^{(l)})^2+\omega^2}(1+2e_{\mu,i}^{(l)}+e_{\mu,i}^{(l)^2})\\
&-\omega\frac{\sin(\Theta_\mu)}{2\pi}A_\mu\sum_{k=1}^{\infty}\frac{P_\mu A_\mu U_\mu^{(k)}\delta G_\mu^{(k)}\lambda_\mu^{(k)}}{(\lambda_\mu^{(k)})^2+\omega^2}(1+2e_\mu^{(k)}+e_\mu^{(k)^2})\\
&-\omega^2\frac{\cos(\Theta_{\mu,i})}{2\pi}\sum_{i=1}^{M}A_{\mu,i}\sum_{l=1}^{\infty}\frac{P_{\mu,i}A_{\mu,i}U_{\mu,i}^{(l)}\delta G_{\mu,i}^{(l)}}{(\lambda_{\mu,i}^{(l)})^2+\omega^2}(1-e_{\mu,i}^{(l)^2})\\
&+\omega^2\frac{\cos(\Theta_\mu)}{2\pi}A_\mu\sum_{k=1}^{\infty}\frac{P_\mu A_\mu U_\mu^{(k)}\delta G_\mu^{(k)}}{(\lambda_\mu^{(k)})^2+\omega^2}(1-e_\mu^{(k)^2})\\
&+\frac{\omega}{4\pi}\sum_{i=1}^{M}A_{\mu,i}\sum_{l=1}^{\infty}\delta G_{\mu,i}^{(l)^2}(1-e_{\mu,i}^{(l)^2})\\
&+\frac{\omega}{4\pi}A_\mu\sum_{k=1}^{\infty}\delta G_\mu^{(k)^2}(1-e_\mu^{(k)^2})\,,\quad\text{where }\Theta_{\mu,i}+\Theta_\mu=\pi\,. \qquad (9.7)
\end{aligned}
$$

In the special case of complete mixing at junctions, the final six summation terms are zero. The final two terms are distinctive in that they do not involve the shear contributions $U_{\mu,i}^{(l)}$, $U_\mu^{(k)}$. When the flow is axisymmetric, it is via these positive-definite junction terms that the non-axisymmetric modes (7.3*a*,*d*) can augment the shear dispersion.

10. Shorter formula for the single-junction shear dispersion

For compactness, we introduce more notational shorthand:

$$
s_\mu^{(k)}=\frac{P_\mu A_\mu U_\mu^{(k)}}{(\lambda_\mu^{(k)})^2+\omega^2}\lambda_\mu^{(k)}\sin(\Theta_\mu)\,,\quad s_{\mu,i}^{(l)}=\frac{P_{\mu,i}A_{\mu,i}U_{\mu,i}^{(l)}}{(\lambda_{\mu,i}^{(l)})^2+\omega^2}\lambda_{\mu,i}^{(l)}\sin(\Theta_{\mu,i})\,, \qquad (10.1a,b)
$$

$$
c_\mu^{(k)}=\frac{P_\mu A_\mu U_\mu^{(k)}}{(\lambda_\mu^{(k)})^2+\omega^2}\omega\cos(\Theta_\mu)\,,\quad c_{\mu,i}^{(l)}=\frac{P_{\mu,i}A_{\mu,i}U_{\mu,i}^{(l)}}{(\lambda_{\mu,i}^{(l)})^2+\omega^2}\omega\cos(\Theta_{\mu,i})\,. \qquad (10.1c,d)
$$

The earlier shorthand (9.6*c*,*d*) can be re-written more symmetrically:

$$
\Delta_\mu^{(k)}=s_\mu^{(k)}(1+e_\mu^{(k)})-c_\mu^{(k)}(1-e_\mu^{(k)})\,,\quad \Delta_{\mu,i}^{(l)}=s_{\mu,i}^{(l)}(1+e_{\mu,i}^{(l)})-c_{\mu,i}^{(l)}(1-e_{\mu,i}^{(l)})\,. \qquad (10.1g,h)
$$

Completing the square in equation (9.7) with respect to $\delta G_{\mu}^{(k)}$ and $\delta G_{\mu,i}^{(l)}$ leads to the comparatively short expression

$$\left\langle \sum_{\mu'} A_{\mu'} S_{\mu'} \right\rangle = \left(\frac{\Theta_{\mu,i}}{\pi} - \frac{\sin(2\Theta_{\mu,i})}{2\pi} \right) \sum_{i=1}^{M} A_{\mu,i} \tilde{S}_{\mu,i}(\omega, \infty)$$
$$- \left(\frac{\Theta_{\mu}}{\pi} - \frac{\sin(2\Theta_{\mu})}{2\pi} \right) A_{\mu} \tilde{S}_{\mu}(\omega, \infty)$$
$$- \frac{\omega}{\pi} \sum_{i=1}^{M} A_{\mu,i} \sum_{l=1}^{\infty} \frac{s_{\mu,i}^{(l)} \Delta_{\mu,i}^{(l)}}{1 - e_{\mu,i}^{(l)}} - \frac{\omega}{\pi} A_{\mu} \sum_{k=1}^{\infty} \frac{s_{\mu}^{(k)} \Delta_{\mu}^{(k)}}{1 - e_{\mu}^{(k)}}$$
$$+ \frac{\omega}{4\pi} \sum_{i=1}^{M} A_{\mu,i} \sum_{l=1}^{\infty} \left(\delta G_{\mu,i}^{(l)} + \frac{\Delta_{\mu,i}^{(l)}}{1 - e_{\mu,i}^{(l)}} \right)^2 (1 - e_{\mu,i}^{(l)2})$$
$$+ \frac{\omega}{4\pi} A_{\mu} \sum_{k=1}^{\infty} \left(\delta G_{\mu}^{(k)} - \frac{\Delta_{\mu}^{(k)}}{1 - e_{\mu}^{(k)}} \right)^2 (1 - e_{\mu}^{(k)2}) . \tag{10.2}$$

For the trivial case of negligible change of area or of velocity profile, we have

$$\delta G_{\mu}^{(k)} = -s_{\mu}^{(k)} - c_{\mu}^{(k)} , \quad \delta G_{\mu,i}^{(l)} = s_{\mu,i}^{(l)} + c_{\mu,i}^{(l)} , A_{\mu,1} = A_{\mu} , \text{and } P_{\mu,1} = P_{\mu} . \tag{10.3a–d}$$

It can be verified from (10.2) that the attenuation terms $e_{\mu}^{(k)}$, $e_{\mu,i}^{(l)}$ cancel exactly and the volumetric shear dispersion agrees with the no-junction result (7.8). Another easy deduction is that the merged channel contribution to the shear dispersion is minimized if

$$\delta G_{\mu}^{(k)} = \frac{\Delta_{\mu}^{(k)}}{1 - e_{\mu,i}^{(l)}} = s_{\mu}^{(k)} \frac{1 + e_{\mu}^{(k)}}{1 - e_{\mu}^{(k)}} - c_{\mu}^{(k)} . \tag{10.4}$$

This condition is distinct from either well-mixed junctions or the trivial case (10.3*a*).

In the limit as the phase at splitting Θ_{μ} tends to zero, the volume-following frame of reference is only in the merged μ channel for a vanishingly small fraction of the flow cycle. Physically this implies that the effective shear dispersion should become independent of the detailed properties of the merged channel as $x \to x_{\mu}$:

$$\left\langle \sum_{\mu'} A_{\mu'} S_{\mu'} \right\rangle = \sum_{i=1}^{M} A_{\mu,i} \tilde{S}_{\mu,i}(\omega, \infty)$$
$$+ \frac{\omega}{4\pi} \sum_{i=1}^{M} A_{\mu,i} \sum_{l=1}^{\infty} \left(\delta G_{\mu,i}^{(l)} + \frac{P_{\mu,i} A_{\mu,i} U_{\mu,i}^{(l)}}{(\lambda_{\mu,i}^{(l)})^2 + \omega^2} \omega \right)^2 (1 - e_{\mu,i}^{(l)2}) . \tag{10.5}$$

At the excursion distance mouthwards of the junction, the volume-following frame of reference only enters the sub-channels for a vanishingly small fraction of the flow cycle. Thus, the effective shear dispersion becomes independent of the detailed properties of the μ, i sub-channels as $x \to x_{\mu} + 2\hat{U}/\omega$:

$$\left\langle \sum_{\mu'} A_{\mu'} S_{\mu'} \right\rangle = A_{\mu} \tilde{S}_{\mu}(\omega, \infty)$$
$$+ \frac{\omega}{4\pi} A_{\mu} \sum_{k=1}^{\infty} \left(\delta G_{\mu}^{(k)} - \frac{P_{\mu} A_{\mu} U_{\mu}^{(k)}}{(\lambda_{\mu}^{(k)})^2 + \omega^2} \omega \right)^2 (1 - e_{\mu}^{(k)2}) . \tag{10.6}$$

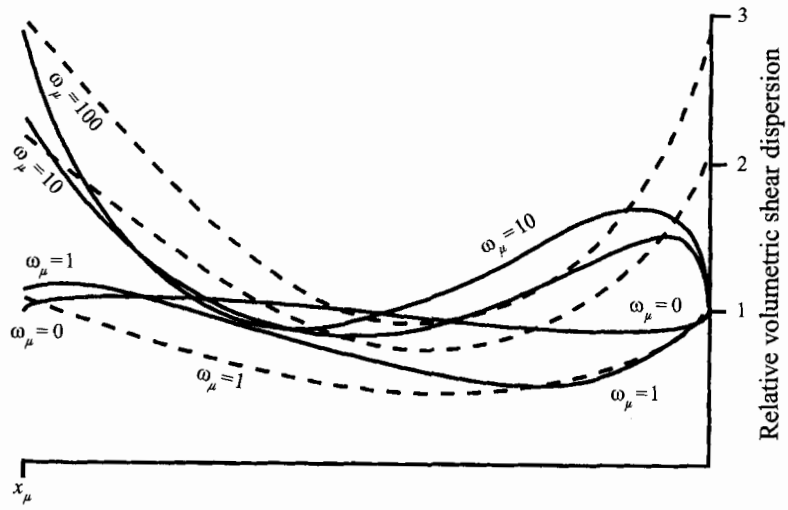

FIGURE 6. Period-averaged, volume-following shear dispersion relative to that of a non-branched oscillatory flow near a Y-junction with all three channels identical. Particle-following matching yields the continuous curves while a well-mixed junction yields the dashed lines.

The final junction-related term is relatively unimportant in the limits of low frequencies $\omega = 0$ and of negligible departure from the uniform channel result (7.8*b*).

11. Low- and high-frequency limits

For low-frequency oscillations, with ω much less than $\lambda_\mu^{(k)}$ or $\lambda_{\mu,i}^{(l)}$, any effect of matching or vigorous mixing at the junctions has a time range of influence short relative to the flow cycle. The volumetric shear dispersion (9.7) is dominated by just the first two terms:

$$\left\langle \sum_{\mu'} A_{\mu'} S_{\mu'} \right\rangle = \frac{[2\Theta_{\mu,i} - \sin(2\Theta_{\mu,i})]}{2\pi} \sum_{i=1}^{M} A_{\mu,i} \widetilde{S}_{\mu,i}(0,\infty) + \frac{[2\Theta_\mu - \sin(2\Theta_\mu)]}{2\pi} A_\mu \widetilde{S}_\mu(0,\infty) \,. \tag{11.1}$$

Thus, there is a transition between the area-weighted sum of the no-junctions results (11.1) either side of the junction. The magnitude of the area-weighted shear dispersion is not just related to the time in each reach, but also depends (5.6) upon the square of the centroid distortion G experienced in each reach . There is not the linear (nor even quadratic) dependence upon Θ_μ, that was exhibited by the effective area (9.3). Mouthward of a junction, the low-frequency volumetric shear dispersion $\widetilde{S}_\mu(0,x)$ does not exhibit a simple linear transition with respect to either Θ_μ or x.

In assessing the combined effect of oscillations and junctions upon the volumetric dispersion, it is appropriate to use the no-junction volumetric shear dispersion (11.1) as a comparator:

$$\frac{\widetilde{S}_\mu(\omega,x)}{\widetilde{S}_\mu(\omega,\infty)} = \left\langle \sum_{\mu'} A_{\mu'} S_{\mu'} \right\rangle \left\{ \left\langle \sum_{\mu'} A_{\mu'} \right\rangle \widetilde{S}_\mu(\omega,\infty) \right\}^{-1} . \tag{11.2}$$

Figure 6 shows results corresponding to the special case studied experimentally by Paloski *et al.* (1987), in which the two sub-channels and the merged channel all have the same areas and decay rates.

The curve labelled $\omega_\mu = 0$ in figure 6 shows the low-frequency results. Although the volumetric shear dispersion for the sub-channels is the same as that for the merged channel, the quotient (11.2) deviates from 1. Close to the junction the volume-following frame of reference is only in the single merged channel near the turn of the flow, when the low-frequency centroid distortion G is small and the diffusion-weighted mean square S_μ is extremely small. Thus, halving the already small contribution to $\langle \sum A_{\mu'} S_{\mu'} \rangle$ does not cause much reduction, but the temporary halving of area lowers $\langle \sum A_{\mu'} \rangle$ more noticeably. Hence, the cycle-averaged volumetric shear dispersion $\tilde{S}_\mu(\omega, x)$ is slightly increased. Conversely, near the excursion distance mouthward from the junction, the volume-following frame of reference only moves into the pair of sub-channels at the other turn of the flow, when the low-frequency centroid distortion G is again small and the squared quantities $S_{\mu,1}$, $S_{\mu,2}$ are extremely small. So doubling a small contribution to $\langle \sum A_{\mu'} S_{\mu'} \rangle$ is not significant by comparison to the doubled area contribution to $\langle \sum A_{\mu'} \rangle$. So near the excursion distance, the cycle-averaged volumetric shear dispersion $\tilde{S}_\mu(\omega, x)$ is decreased.

As the frequency increases, ω exceeds $\lambda_{\mu,i}^{(l)}$ or $\lambda_\mu^{(k)}$ for more and more of the modes. The formal limiting version of (10.2) for high frequencies is

$$\begin{aligned}\left\langle \sum_{\mu'} A_{\mu'} S_{\mu'} \right\rangle = {} & \left(\frac{\Theta_\mu}{2\pi} - \frac{\sin(2\Theta_\mu)}{4\pi} - \frac{\sin(\Theta_\mu)^2}{\pi \Theta_\mu} \right) A_\mu \sum_{k=1}^{\infty} (P_\mu A_\mu U_\mu^{(k)})^2 \frac{\lambda_\mu^{(k)}}{\omega^2} \\ & + \left(\frac{\Theta_{\mu,i}}{2\pi} - \frac{\sin(2\Theta_{\mu,i})}{4\pi} - \frac{\sin(\Theta_{\mu,i})^2}{\pi \Theta_{\mu,i}} \right) \sum_{i=1}^{M} A_{\mu,i} \sum_{l=1}^{\infty} (P_{\mu,i} A_{\mu,i} U_{\mu,i}^{(l)})^2 \frac{\lambda_{\mu,i}^{(l)}}{\omega^2} \\ & + \frac{\Theta_{\mu,i}}{\pi} \sum_{i=1}^{M} A_{\mu,i} \sum_{l=1}^{\infty} \lambda_{\mu,i}^{(l)} \left(\delta G_{\mu,i}^{(l)} + \left[\frac{\sin(\Theta_{\mu,i})}{\Theta_{\mu,i}} - \cos(\Theta_{\mu,i}) \right] \frac{P_{\mu,i} A_{\mu,i} U_{\mu,i}^{(l)}}{\omega} \right)^2 \\ & + \frac{\Theta_\mu}{\pi} A_\mu \sum_{k=1}^{\infty} \lambda_\mu^{(k)} \left(\delta G_\mu^{(k)} - \left[\frac{\sin(\Theta_\mu)}{\Theta_\mu} - \cos(\Theta_\mu) \right] \frac{P_\mu A_\mu U_\mu^{(k)}}{\omega} \right)^2 . \end{aligned} \tag{11.3}$$

The top curves in figure 6 (labelled $\omega_\mu = 100$) illustrate the high-frequency behaviour. By contrast to the low-frequency limit (11.1), there is strong dependence upon the nature of the matching, even at the two end points $\Theta_{\mu,i} = \pi$ and $\Theta_\mu = \pi$. By re-starting the dispersion process, vigorous mixing at junctions can make the centroid displacement be systematically one-signed (rather than oscillate about zero) with an increased mean square, i.e. larger shear dispersion (5.6). Over the transition regime the average dispersion at high frequencies is about twice that of a non-branching flow.

12. Strong attenuation matching

A less severe use of the low-frequency or narrow-channel assumption, is to simplify the determination of the matching (9.5). On a two-cycle excursion (beginning at the μ junction, (i) going mouthwards into the μ channel, (ii) continuing away from the mouth into the μ, i sub-channel, (iii) returning into the μ channel, (iv) then away from the mouth into the μ, I sub-channel, (v) and finally reaching the μ junction

for a fifth time) the product attenuation would be $e_{\mu}^{(k)}e_{\mu,i}^{(l)}e_{\mu}^{(K)}e_{\mu,I}^{(L)}$. We shall assume that this product is very small for all combinations of routes and modes i,k,l,I,K,L. Equivalently, we assume that $\omega < 4\pi\lambda_{\mu}^{(k)}$ and $\omega < 4\pi\lambda_{\mu,i}^{(l)}$. In this situation, the periodic matching (9.5) has the approximate solution

$$[1-\alpha]\delta G_{\mu}^{(k)} = -\sum_{i=1}^{M}\sum_{l=1}^{\infty} E_{\mu,i}^{(k,l)}\left(\Delta_{\mu,i}^{(l)} - e_{\mu,i}^{(l)}\sum_{m=1}^{\infty} F_{\mu,i}^{(m,l)}\Delta_{\mu}^{(m)}\right), \tag{12.1a}$$

$$[1-\alpha]\delta G_{\mu,i}^{(l)} = \sum_{k=1}^{\infty} F_{\mu,i}^{(k,l)}\left(\Delta_{\mu}^{(k)} - e_{\mu}^{(k)}\sum_{j=1}^{M}\sum_{n=1}^{\infty} E_{\mu,j}^{(k,n)}\Delta_{\mu,j}^{(n)}\right), \tag{12.1b}$$

with

$$\alpha = \sum_{i=1}^{M}\sum_{k=1}^{\infty}\sum_{l=1}^{\infty} F_{\mu,i}^{(k,l)}E_{\mu,i}^{(k,l)}e_{\mu}^{(k)}e_{\mu,i}^{(l)}. \tag{12.1c}$$

The first summation term on the right-hand side of equations (12.1*a,b*) represents the transmission of the non-branching centroid displacement profile across the junction. The second summation term allows for the attenuation experienced since the previous crossing, which may have been relatively recent. The α-term accommodates a further return journey. In some simple cases $[1-\alpha]$ is the determinant for solving the periodic matching linear equations (9.5) and the solutions (12.1*a,b*) are then exact.

Over the full extent of the strong attenuation regime, the functions $f_{\mu}^{(k)}$, $f_{\mu,i}^{(l)}$ defined in equation (7.8*b*) decrease in value by a factor of $16\pi^2$. Thus, any influence of $\delta G_{\mu}^{(k)}$ and $\delta G_{\mu,i}^{(i)}$ upon the cycle-averaged shear dispersion will have become slight within the region of validity of the explicit expressions (12.1*a,b*).

13. Cosine velocity profile

For clarity of exposition, it is desirable that the particle-following matching across junctions should be achieved analytically rather than numerically. Unfortunately, for the merging of two circular cylindrical tubes with Poiseuille pipe flow (appropriate for smaller airways in the lungs), there would seem to be no alternative to a fully computational matching. For the quadratic-velocity-profile plane Poiseuille flow the particle-following matching involves the real root of a cubic equation which can be written explicitly. This section gives an estuarial example in which the matching is even more elementary.

We shall neglect z-dependence, take the depth H to be constant across the flow and we specify cosine velocity and constant diffusivity profiles:

$$u = \tfrac{1}{2}\pi\cos\left(\tfrac{1}{2}\pi y\right)\bar{u}\ ,\ \kappa_2 = \bar{\kappa}\ ,\ m_1 = 1\ ,\ m_2 = B\ ,\ m_3 = H\ . \tag{13.1a–e}$$

In any individual channel μ the width, depth, velocity and diffusivity scales B, H, $\hat{U}$, $\bar{\kappa}$ are assumed to be constant. Such a flow might be associated with a dredged channel for which increasing vegetation towards the sides slows the flow. The modes are the same and the velocity profile is similar to plane Poiseuille flow.

The eigenmodes are trigonometric functions, with only even modes contributing to

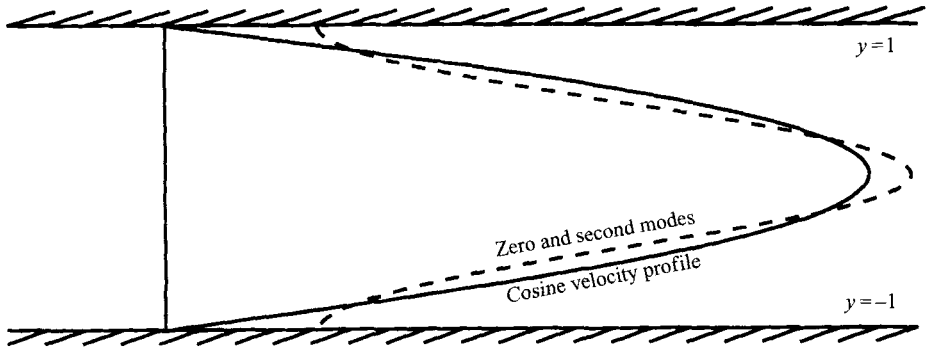

FIGURE 7. Cosine velocity profile and its zero plus second mode approximation.

the even velocity profile:

$$\psi^{(2N+1)}(y) = \sqrt{2}\sin\left(\left(N+\tfrac{1}{2}\right)\pi y\right)\ ,\quad \psi^{(2N)}(y) = \sqrt{2}\cos(N\pi y)\ , \tag{13.2a,b}$$

$$\lambda^{(2N+1)} = \frac{\left(N+\frac{1}{2}\right)^2\pi^2\bar{\kappa}}{B^2}\ ,\quad \lambda^{(2N)} = \frac{N^2\pi^2\bar{\kappa}}{B^2}\ ,\quad u^{(2N)} = \frac{\sqrt{2}(-1)^{N+1}}{4N^2-1}\hat{U}\ . \tag{13.2c–f}$$

The first odd mode $\psi^{(1)}$ is the counterpart to the non-axisymmetric modes (7.3) for circular cylindrical tubes, in that it can arise only as a result of matching at the junctions. In the absence of branching, the formula (7.8*c*) for the shear dispersion and the corresponding single-term approximation are

$$\langle D\rangle = \frac{B^2\hat{U}^2}{\bar{\kappa}\pi^2}\sum_{N=1}^{\infty}\frac{N^2}{(4N^2-1)^2[N^4+(\omega B^2/\bar{\kappa}\pi^2)^2]} \sim \frac{B^2\hat{U}^2}{\bar{\kappa}\pi^2}\frac{1}{9[1+(\omega B^2/\bar{\kappa}\pi^2)^2]}\ . \tag{13.3}$$

The next ($N = 2$) term is smaller by a factor of 200 than the $N = 1$ term. Figure 7 shows that just the zero (uniform) and $\psi^{(2)}$ modes also suffice to approximate the velocity profile.

The crucial property of this model problem is that the particle-following matching can be performed explicitly. We introduce an asymmetry parameter ϕ such that fractions $(1+\phi)/2$ and $(1-\phi)/2$ of the volume flux go into the $\mu,1$ and $\mu,2$ sub-channels. The particle-following matching (3.5) has the explicit form

$$Y^{-}_{\mu,1} = \frac{2}{\pi}\arcsin\left(\frac{2}{1+\phi}\sin\left(\tfrac{1}{2}\pi y_\mu\right)+\frac{1-\phi}{1+\phi}\right) \text{ for } -1 \leqslant y_\mu \leqslant \frac{2}{\pi}\arcsin(\phi)\ , \tag{13.4a}$$

$$Y^{-}_{\mu,2} = \frac{2}{\pi}\arcsin\left(\frac{2}{1-\phi}\sin\left(\tfrac{1}{2}\pi y_\mu\right)-\frac{1+\phi}{1-\phi}\right) \text{ for } \frac{2}{\pi}\arcsin(\phi) \leqslant y_\mu \leqslant 1\ , \tag{13.4b}$$

$$Y^{+}_{\mu,1} = \frac{2}{\pi}\arcsin\left(\frac{1+\phi}{2}\sin\left(\tfrac{1}{2}\pi y_{\mu,1}\right)-\frac{1-\phi}{2}\right)\ , \tag{13.4c}$$

$$Y^{+}_{\mu,2} = \frac{2}{\pi}\arcsin\left(\frac{1-\phi}{2}\sin\left(\tfrac{1}{2}\pi y_{\mu,2}\right)+\frac{1+\phi}{2}\right)\ . \tag{13.4d}$$

If we make a two-mode truncation by including only the unforced first mode and the forced second mode, then there are eight $F^{(k,l)}_{\mu,i}$ and eight $E^{(k,l)}_{\mu,i}$ flood and ebb

matching coefficients to be evaluated. First we note that for the lower $\mu, 1$ sub-channel

$$\psi^{(1)}(Y^{+}_{\mu,1}) = \sqrt{2}\left(-\frac{(1-\phi)}{2} + \frac{1+\phi}{2}\sin\left(\tfrac{1}{2}\pi y_{\mu,1}\right)\right), \tag{13.5a}$$

$$\psi^{(2)}(Y^{+}_{\mu,1}) = \sqrt{2}\left(\frac{1+2\phi-3\phi^2}{4} + (1-\phi^2)\sin\left(\tfrac{1}{2}\pi y_{\mu,1}\right) + \frac{(1+\phi)^2}{4}\cos(\pi y_{\mu,1})\right), \tag{13.5b}$$

$$\psi^{(1)}(Y^{-}_{\mu,1}) = \frac{\sqrt{2}}{1+\phi}\left(1-\phi+2\sin\left(\tfrac{1}{2}\pi y_{\mu}\right)\right) \text{ for } -1 \leqslant y_{\mu} \leqslant \frac{2}{\pi}\arcsin(\phi), \tag{13.5c}$$

$$\psi^{(2)}(Y^{-}_{\mu,1}) = \frac{\sqrt{2}}{(1+\phi)^2}\left(-5+6\phi-\phi^2-8(1-\phi)\sin\left(\tfrac{1}{2}\pi y_{\mu}\right)+4\cos(\pi y_{\mu})\right). \tag{13.5d}$$

The integrals (8.2) for the $\mu, 1$ matching coefficients can be evaluated explicitly:

$$F^{(1,1)}_{\mu,1} = \frac{1+\phi}{2}, \; F^{(1,2)}_{\mu,1} = 0, \; F^{(2,1)}_{\mu,1} = (1-\phi^2), \; F^{(2,2)}_{\mu,1} = \frac{(1+\phi)^2}{4}, \tag{13.6a–d}$$

$$E^{(1,1)}_{\mu,1} = \frac{\pi + 2\arcsin(\phi) - 2(1-\phi^2)^{1/2}}{\pi(1+\phi)}, \; E^{(2,1)}_{\mu,1} = \frac{2}{3\pi}(2+\phi)(1-\phi^2)^{1/2}, \tag{13.6e,f}$$

$$E^{(1,2)}_{\mu,1} = \frac{-12(1-\phi)[\pi + 2\arcsin(\phi)] + 2(19-6\phi+\phi^2)(1-\phi^2)^{1/2}}{3\pi(1+\phi)^2}, \tag{13.6g}$$

$$E^{(2,2)}_{\mu,1} = \frac{6[\pi + 2\arcsin(\phi)] - 2(8+\phi-2\phi^2-\phi^3)(1-\phi^2)^{1/2}}{3\pi(1+\phi)^2}. \tag{13.6h}$$

Graphs of these $\mu, 1$ matching coefficients as functions of ϕ were shown in figures 3 and 4. Symmetry considerations allow us to deduce the corresponding $\mu, 2$ matching coefficients:

$$F^{(k,l)}_{\mu,2}(\phi) = (-1)^{k+l}F^{(k,l)}_{\mu,1}(-\phi), \; E^{(k,l)}_{\mu,2}(\phi) = (-1)^{k+l}E^{(k,l)}_{\mu,1}(-\phi), \tag{13.7a,d}$$

14. Numerical examples

Here we use the two-mode truncation for the cosine velocity profile, to calculate the results already displayed in figures 3, 4 and 6. For simplicity, we take the junction to be symmetric $\phi = 0$. By virtue of the symmetry there is much exact cancelling between the contributions from the sub-channels, in particular $G^{(1)}_{\mu} = 0$. The contributing matching coefficients have the values

$$F^{(2,1)}_{\mu,1} = 1, \; F^{(2,2)}_{\mu,1} = \frac{1}{4}, \; E^{(2,1)}_{\mu,1} = \frac{4}{3\pi} = 0.4244, \; E^{(2,2)}_{\mu,1} = 2 - \frac{16}{3\pi} = 0.302. \tag{14.1a–d}$$

The $F^{(2,1)}_{\mu,1}$ coefficient has a suitably large value to generate a noticeable contribution in the $l = 1$ mode. To characterize the influence of flow oscillations we define a dimensionless frequency parameter:

$$\omega_{\mu} = \frac{\omega B^2_{\mu}}{\bar{\kappa}_{\mu}\pi^2}. \tag{14.2}$$

For the first example, the sub-channels are specified as having areas and decay rates identical to those of the merged channel ($A_{\mu,i} = A_{\mu}$, $\lambda^{(2)}_{\mu,i} = \lambda^{(2)}_{\mu}$) as in the experiments of Paloski *et al.* (1987).

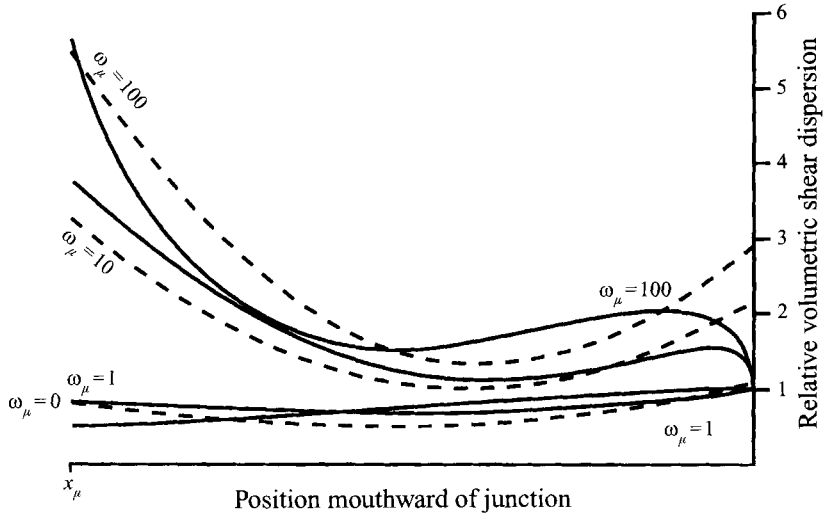

FIGURE 8. Cycle-averaged, volume-following shear dispersion relative to the non-branched case when sinusoidal flow in branches with relative areas 1/2 merge at a Y-junction. Particle-following matching yields the continuous curves while a well-mixed junction yields the dashed lines.

For a given low-tide (minimum lung volume) position x within an excursion distance of a junction x_μ, we first use (9.2) to determine the phase angle Θ_μ^- at which the volume-following frame of reference reaches the junction. The shorthand notation definitions (9.6), (10.1) allow us to evaluate the attenuations $e_\mu^{(2)}$, $e_{\mu,1}^{(1)}$, $e_{\mu,1}^{(2)}$ and the forced amplitude terms $A_\mu^{(2)}$, $s_\mu^{(2)}$, $A_{\mu,1}^{(2)}$, $s_{\mu,1}^{(2)}$. In the vigorous mixing case, we then have enough information to evaluate the six-term formula (10.2) or the numerically more robust first eight terms of the formula (9.7). Summations over the sub-channels merely require a doubling of the $\mu, 1$ contribution. If the mixing is not vigorous, then the strong-attenuation approximation (12.1) gives the starting values for the centroid displacement function amplitudes either side of the junction $\delta G_\mu^{(2)}$, $\delta G_{\mu,1}^{(1)}$ and $\delta G_{\mu,1}^{(2)}$.

Figure 6 compares the dimensionless shear dispersion (11.2) for well-mixed junctions and for the particle-following matching (14.1) when the dimensionless frequency has the values $\omega_\mu = 0, 1, 10, 100$. For well-mixed junctions (dashed curves) the dispersion at low frequencies is reduced but at high frequencies rises far above the no-junction value, particularly near the junction and near the excursion distance. For particle-following matching (continuous curves) the increase in dispersion at low frequencies can be linked to the presence of the non-symmetric $l = 1$ mode. At the excursion distance the particle-following matching nearly adjusts to the no-junction value. The inclusion of more modes would allow short scale adjustments to be more accurately represented.

As a second numerical example, we consider a junction at which the total flow area remains constant $A_{\mu,1} + A_{\mu,2} = A_\mu/2$. The sub-channels are assumed to have areas half and decay rates twice those of the merged channel ($\lambda_{\mu,i}^{(2)} = 2\lambda_\mu^{(2)}$). In figure 8 the greater increase in shear dispersion with increasing frequency near the junction than near the excursion distance, is related to the increase with frequency of the dispersion in the sub-channel relative to the merged-channel reference dispersion $\tilde{S}_\mu(\omega, \infty)$. On average throughout the junction-affected region the shear dispersion can be more than doubled relative to a non-branched flow.

15. Suggestions for further work

It is the synchronism assumption for the leading-order flow in adjacent sub-channels that permits the use of a volume-following frame of reference. In that moving frame, shear dispersion in branched oscillatory flows could be presented as an extension of long established theory (Taylor 1953) for unbranched steady flows. Branching contributes to distortions across the flow (the volumetric centroid displacement function) and hence increases the shear dispersion (5.6). Non-synchronous ventilation (Schijf & Schonfeld 1953) deserves further theoretical and experimental investigation if only to demarcate the regimes in which synchronous and non-synchronous dispersion dominate.

At several stages in the above calculations, selections were made for clarity of exposition. For example, branching need not be symmetric. For the cosine velocity with the two-mode truncation, all the necessary coefficients have been evaluated (13.6). The odd 1 mode in the merged channel, which is absent in the symmetric case, might cause qualitative changes from figures 6 and 8. Also, when secondary flows are important (Pedley & Kamm 1987) the selection of modes used in § 7 is not appropriate. In particular, the eigenvalues, the consequent high- / low-frequency demarcation and the scaling laws for the reference value of the volumetric shear dispersion coefficient (unaffected by branching), would be dependent upon the strength of the secondary flows.

Breathing involves air movement over many generations of the branching flow. The experiments of Paloski *et al.* (1987) allowed up to two generations movement. It would be straightforward to extend the results (9.3), (10.2) to accommodate a sinusoidal flow crossing many junctions. The matching (12.1) would also have to be extended. It is tempting to speculate that multiple junctions would give enhanced dispersion beyond that exhibited in figures 6 and 8 and towards the factor of 3 increase as observed by Paloski *et al.* (1987).

As noted in §13, the particle-following matching for lungs would require numerical solution for the Poiseuille pipe flow as it adjusts from two sub-channels to a single channel. This would allow the integrals (8.2) for the matching coefficients to be evaluated numerically.

One facet of the many studies of high-frequency ventilation has concerned the effects upon gaseous exchange of waveform asymmetry between inhalation and exhalation. Most of the present paper allows for arbitrary periodic time dependence. In a two-mode truncation it would be tractable to explore non-sinusoidal flows.

For blood oxygenators, vigorous mixing destroys the red blood corpusles. Yet to oxygenate efficiently, it is desirable to minimize longitudinal spread. The criterion (10.4) may help in the design of suitable oscillatory branched flows, e.g. in selecting the flow-splitting ratio and channel sizes which minimize the total spread at a given frequency. Similar considerations arise in chemical engineering applications.

The focus of this paper has been upon the evaluation of the volumetric shear dispersion rather than upon its solution of the drift-diffusion equation (6.6). Recently, Bressloff, Dwyer & Kearney (1996*a*, *b*) have given explicit methods for the construction of point-release solutions for drift-diffusion on branched networks (trees) with identical constant-coefficient branches of arbitrary lengths and connectivities. Their modified Gaussian solutions quantify how a point tracer release at an interior position permeates into accessible branches. It would be useful if the methods derived by Bressloff *et al.* (1996*a*) could be generalized to non-constant coefficients and applied to the model derived here (6.6) for transport in lungs and branched estuaries.

I wish to thank Tim Pedley and Roger Kamm for their patient encouragement. Helpful comments from the referees removed some obscurities.

REFERENCES

ADLER, P. M. 1985 Transport processes in fractals – III. Taylor dispersion in two examples of fractal capillary networks. *Intl J. Multiphase Flow* **11**, 241–254.

BOHN, D. J., MIYASAKA, K., MARCHAK, B. E., THOMPSON, W. K., FROESE, A. B. & BRYAN, A. C. 1980 Ventilation by high frequency oscillation. *J. Appl. Physiol.* **48**, 710–716.

BRESSLOFF, P. C., DWYER, V. M. & KEARNEY, M. J. 1996*a* A "sum-over-path" approach to diffusion on trees. *J. Phys.* A **29**, 1881–1895.

BRESSLOFF, P. C., DWYER, V. M. & KEARNEY, M. J. 1996*b* Green's function of the drift-diffusion equation on a tree. *J. Phys.* A (submitted).

CHATWIN, P. C. 1975 On the longitudinal dispersion of passive contaminant in oscillatory flows in tubes. *J. Fluid Mech.* **71**, 513–527.

DAISH, N. C. 1985 Shear dispersion problems in open-channel flows. PhD thesis, Cambridge University.

PALOSKI, W. H., SLOSBERG, R. B. & KAMM, R. D. 1987 Effect of gas properties and waveform asymmetry on gas transport in a branching tube network. *J. Appl. Physiol.* **62**, 892–901.

PEDLEY, T. J. & KAMM, R. D. 1988 The effect of secondary motion on axial transport in oscillatory tube flow. *J. Fluid Mech.* **193**, 347–367.

ROSSING, T. H., SLUTSKY, A. S., LEHR, J., DRINKER, P., KAMM, R. D. & DRAZEN, J. M. 1981 Tidal volume and frequency dependence of carbon dioxide elimination by high frequency ventilation. *N. Engl. J. Med.* **305**, 1375–1379.

SAFFMAN, P. G. 1969 A mathematical treatment of dispersion in flow through a branching tree. In *Circulatory and Respiratory Mass Transport* (ed. G. E. W. Wolstenholme & J. Knight), pp. 298–301. J & A Churchill Ltd.

SCHIJF, J. B. & SCHONFELD, J. C. 1953 Theoretical considerations on the motion of salt and fresh water. *Proc. Minnesota Intl Hydraul. Conf., Minneapolis*, pp. 321–333.

SHINOHARA, K., TSUBAKI, T., AWAYA, Y. & FURUMOTO, K. 1969 Numerical analysis on the salinity intrusion in the tidal estuary of well-mixed type. *Proc. 13th Cong. IAHR, Kyoto, Japan*, vol 3, pp. 165–172.

SMITH, R. 1977 Long-term dispersion of contaminants in small estuaries. *J. Fluid Mech.* **82**, 129–146.

SMITH, R. 1995 Effect of islands upon dispersion in rivers. *J. Fluid Mech.* **292**, 249–270.

TAYLOR, G. I. 1953 Dispersion of soluble matter in solvent flowing slowly through a tube. *Proc. R. Soc. Lond.* A **219**, 186–203.

ULTMAN, J. S. & BLATMAN, H. S. 1977 A compartmental model for the analysis of mixing in tube networks. *AIChE J.* **23**, 169–176.

WATSON, E. J. 1983 Diffusion in oscillatory pipe flow. *J. Fluid Mech.* **133**, 233–244.